Revision 2

Quartz nanocrystals in the 2.48-Ga Dales Gorge banded iron formation of Hamersley, Western Australia

Yi-Liang Li[1,*], David R. Cole[2], Kurt Konhauser[3], Lung Sang Chan[1]

[1] Department of Earth Sciences, The University of Hong Kong, Hong Kong

[2] School of Earth Sciences, Ohio State University, Columbus, OH 43210, USA

[3] Department of Earth and Atmospheric Sciences, The University of Alberta, Edmonton, Alberta, T6G 2E3, Canada

* Corresponding author:

E-mail: yiliang@hku.hk

ABSTRACT

Banded iron formations (BIF) have recently been used as proxies for tracking the chemical changes associated with the transition from an anoxic to oxic atmosphere around 2.48 billion years ago, known as the Great Oxidation Event (GOE). The timing of GOE has been ascribed to both the collapse of a methane greenhouse and a decreased overall demand for oxygen due to the production of more oxidizing gases associated with greater subaerial volcanism. The latter is a byproduct of a period of high mantle plume activity and the formation of new continental crust between 2.51 to 2.45 Ga. Here we report unique mineral evidence for momentary subaerial volcanism recorded in hematite-rich layers of the 2.48 Ga BIF from Dales Gorge, Hamersley of Western Australia. The BIF contains euhedral quartz nanocrystals (QNC) which only occur on the surfaces or in cavities of hematite breccias exhibiting soft-sediment features and exogenous source. These QNCs with an average size of 170±100 nm are distinct to the amorphous chert of the BIF mineral assemblage and have the smallest crystal sizes of well-crystallized quartz ever reported. We suggest that QNCs represent pyroclastic materials that were transported as dust particles to the BIF depositional setting. Although the analysis of one specific BIF unit does not provide proof of changing modes of

volcanism during the Archean-Paleoproterozic transition, this high resolution petrological study does confirm that subaerial volcanism existed at that time.

Keywords: banded iron formation; chert; quartz nanocrystal; subaerial volcanism; rise of atmospheric oxygen.

INTRODUCTION

Superior-type banded iron formations are layered chemical precipitates that developed in near-shore continental shelf environments and are typically interbedded with carbonates and black shales. Banding can be observed on a wide range of scales, from coarse macrobands (meters in thickness) to mesobands (centimeter-thick units) to millimeter and submillimeter layers (Trendall & Blockley, 1970). Amongst the macrobands, the layers are commonly subdivided on the basis of mineralogy, with “BIF” macrobands dominated by iron oxides (e.g., hematite, magnetite) and chert or carbonate (siderite, dolomite-ankerite) and “S” macrobands comprising chert-carbonate-silicate BIF interspersed with shaley horizons (Morris, 1993). The BIF macrobands are widely accepted as being chemical precipitates, formed initially of a mixture of ferric hydroxide [$Fe(OH)_3$], greenalite [$Fe_3Si_2O_5(OH)_4$], siderite ($FeCO_3$), and amorphous silica ($SiO_2 \cdot nH_2O$) (e.g., Klein, 2005); these primary minerals have since been modified by both diagenetic and metamorphic processes. By contrast, the S macrobands, such as in the 2.48-Ga Penge Iron Formation South Africa, are believed to have been deposited when clastic materials were transported during a sea level drop into what was previously a sediment-starved, chemical precipitation environment (Bau and Dulski, 1996).

Interestingly, in the 2.48 Gyr Dales Gorge Member of the Brockman Iron Formation, Western Australia, the S macrobands have instead been suggested to have been derived from subaerial pyroclastic input on normal BIF chemical processes. The S macrobands contain about 40-45% shale, which is made up of stilpnomelane and chlorite, with varying amounts of feldspar, mica, quartz, carbonates, carbonaceous material and sulfides. A volcanogenic origin to the shales was proposed based on their lateral stratigraphic continuity and chemical composition (Trendall and Blockley, 1970; Ewers and Morris, 1981), although the only direct evidence of pyroclastic material is a few putative volcanic shards (La Berge, 1966). During S macroband accumulation, total annual silica precipitation increased, as did the ratio of silica to iron. This increase has been attributed to surface cooling associated with "volcanic winters", and hence of supersaturation of warm incoming silica saturated water (Morris, 1993).

The potential presence of pyroclastic material in the Dales Gorge BIF also has significant implications for global tectonic evolution during the Late Archean to early Palaeoproterozoic and the rise of atmospheric oxygen. A number of studies have suggested that extensive igneous activity and the rapid growth of continents led to the change of atmospheric redox conditions and consequently the irreversible oxidation of the atmosphere (e.g., Kasting et al. 1993; Kump et al., 2001; Barley et al., 2005; Holland, 2006). Specifically, Kump & Barley (2007) proposed that the transition from extensively submarine to a subaerial volcanism within a narrow time window around 2.5 Ga might have changed the atmospheric composition and favored the stability of free O_2. Campbell & Allen (2008) supported the important role of supercontinent formation but stressed that the accelerated erosion of mountains provided more nutrients for photosynthesis and led to a high burial rate of organic matter, which in turn, allowed for atmospheric O_2 levels to increase.

In light of the importance of the Archean-Paleoproterozoic transition in terms of the evolution of Earth’s surface system, we investigated core samples from the Dales Gorge Member (Li et al., 2011). The BIF has been extensively described in terms of its age, petrology, chemical composition and likely depositional environment (e.g., Trendall and Blockley, 1970; Ewers and Morris, 1981; Morris, 1993; Pickard, 2002; Trendall et al., 2004; Pecoits et al., 2009), but as far as we are aware, no high resolution studies have been conducted on its mineralogy and texture. In this study, we show that a component of quartz in the BIF was likely pyroclastic in nature, supporting the contention that subaerial volcanism existed at that time.

METHODS

For the observation of hematite bands in BIF, samples were ground to μm-sizes and immersed in water to make a hematite suspension. The silica fraction and magnetite crystals were separated either by their rapid setting or response to a permanent magnet. Fine-grained hematite particles collected from the suspension were observed by Hitachi S-4800 FEG scanning electron microscope (SEM) under secondary electron (SE) mode at low voltage (3-5 kV) for surface structures. As the BIFs are mostly made of micro- to nanometer scaled minerals with their textural structures prone to be altered quickly by interaction with liquid, such as water, we also produce fresh surface without any treatment for direct observation. To do so, the cm-scaled specimens were polished to a surface roughness of ~200 nm and then bladed the edge with a screwdriver to peel off thin flakes that produced concoidal, concave surfaces for immediate and direct observation under scanning electron microscopes to avoid contamination. These samples were observed with backscatter electron (BSE) mode for interrogation of electron density heterogeneities which differentiates mineralogical texture features. The chemical compositions were determined by energy dispersive X-ray spectroscopy (EDS) at 20 kV. To extract the ultrafine siliceous minerals incorporated in hematite, the latter was treated by 6M-HCl overnight to dissolve iron oxides completely; the relics were then washed by pure water and dried at room temperature. The Tecnai G2 20 S-TWIN transmission electron microscope (STEM) equipped with EDS was used to characterize the structures of ultrafine minerals

This is a preprint, the final version is subject to change, of the American Mineralogist (MSA)
Cite as Authors (Year) Title. American Mineralogist, in press.
(DOI will not work until issue is live.) DOI: http://dx.doi.org/10.2138/am.2013.4205

by selected area electron diffraction (SAED) along with the observation of morphology and the measurement of chemical composition.

RESULTS

In the BIF sample, the thicknesses of silica bands range from meter-scaled macrobands to micron-scaled microbands that alternate with hematite-rich microbands (Trendall 2002). Figure 1A shows a BSE image of chert (dark in color) and alternating hematite microbands along with disseminated magnetite crystals. The chert was actually made of tightly compacted polyhedrons of several micrometers in size without admixtures of other minerals (Fig.1B). The SE mode image of anhedral hematite reveals μm-sized depressions on the surface (Fig. 1C) made probably by the coexisting minerals of μm-scales. The *in situ* observation of the hematite bands in BSE mode also shows the existence of embedded μm-size chert nodules (black dots, Fig.1D). Under high resolution, some hematite particles are platy hexahedrons of a few μm in size with straight boundaries between particles (Fig. 1E). In the same sample, anhedral hematite also appears in eroded-landform feature (Fig. 1F). The high resolution STEM observation shows single hematite crystals of around 3-5 nm (Fig.2A) with a SAED determined rhombohedral hematite structure ($R\bar{3}C$) (Fig.2B).

Remarkable features preserved in hematite of Dales Gorge BIF are quartz nanocrystals (QNC). QNCs are observed in two modes: (a) as single crystals occupying either in very shallow pits (Fig. 3A, B) or within more developed pits or impact-like depressions with grooves or scratches (Fig. 3C, D, E); and (b) cavities with one or two QNCs inside (Fig.3F, G-L). Figure 3G shows dense QNCs and empty pits scattered on the surface of hematite. Figures 3(H, I & J) show surfaces of hematite with cavities either containing QNCs or remaining empty; Particularly, Fig.3K demonstrates episodic QNC deposition by having QNCs in the lower-left part but without QNC in its upper-right part. Occasionally, small flake-like inclusions of ~120 nm can also be observed adjacent to QNCs (Fig.3L). A statistical assessment of 70 QNC yields an average of 170±100 nm for the long axis of particles and an average of 200±100 nm for the long-axis of associated pits. EDS analysis of a hematite breccia containing a QNC (Fig.4A) shows only a weak peak of Si besides Fe and O peaks, implying a Si-O composition (Fig.4B); comparably, signal of Si cannot be detected on the surface far from these quartz grains. The ~120 nm flakes (Fig.3K, Fig.4C) are rare but is the second mineral that can be found in hematite. A weak Al shoulder peak (Fig. 4D) is shown without any other detectable metal as measured by EDS (detection limit is 0.1% atomic ratio). Because of the extremely low abundance of the flake-like mineral, its mineralogy cannot be determined by STEM. It may be the same Al-bearing phase previously suggested by Ahn & Buseck (1990) and Pecoits et al. (2009) to be Al on the structure of hematite. A STEM observed QNC grain of ~250 nm from the residues of 6M-HCl treated hematite (Fig.5A, bottom right) was further confirmed by SAED to be quartz in structure (Fig. 5B). The euhedral feature (Fig.3B-F) and the periodical structure (Fig.5B) of these QNC particles distinguish their crystallographic habits from the abundant chert in BIFs. The chert from the residue of 6M-HCl treated hematite appear to be microcrystallites that show much smaller sizes than those of QNCs (Fig. 5C) with their average size of 32±12 nm under STEM. These microcrystallites under high resolution STEM can only show diffuse circles by SAED (Fig.5D), indicating long-range disorder which is quite different from QNCs.

QNCs were only observed in the 2.48-Ga Dales Gorge BIF samples as we examined so far. The hematite from randomly selected BIFs of 3.0 Ga from Zimbabwe (Fedo & Eriksson, 1996), 3.0-3.3 Ga of Fig Tree Group, Barberton of South Africa (Eriksson, 1983), 2.52 Ga from North China (Zhai & Windley, 1990), 2.4 Ga from Brazil (Klein and Ladeira, 2000), 1874 Ma from Michigan (Schneider et al., 2000), and 1.8 Ga from North China (Zhai & Windley, 1990) all were devoid of

QNC (Fig.6A-F). No QNCs could be found from the rest part of the mineral assemblages of the above-listed BIF samples.

DISCUSSION

In the entire BIF-assemblage, QNCs and (Si, Al)-containing flakes are the only minerals that can be found in hematite; all the other minerals, namely, magnetite, ferro-carbonate, minnesotaite, chert and occasionally stilpnomelane are at least several micrometers in size and have sharp boundaries to hematite breccias. The ultrafine crystals of hematite (Fig.2) and amorphous chert (Fig.5C-D) indicate the preservation of their early precipitating conditions (Ahn and Buseck, 1990; Knauth, 2005) and these observations also support that QNCs and (Si, Al)-containing flakes were originally deposited at the same time as the precursor of the nano-hematite. The fact that QNCs only found in hematite breccias implies a hiatus between the deposition of hematite and those well crystallized BIF-minerals which all contain Fe^{2+} in their structures. The hematite crystals occur only as ~3-5 nm grains (Fig.2A; Ahn & Buseck, 1990) suggests that when these QNCs were deposited, the original oxyhydroxide, such as $Fe(OH)_3$ had transformed to hematite before consolidation (e.g., Krapež et al., 2003) because the transformation of mineral structures could alter or eliminate the observed "soft-sedimentary" fine structures.

Though hydrodynamically transported terrigenous sediments are absent (Ewers and Morris, 1981; Trendall 2002), the occurrence of nano-quartz airborne "dusts", such as those from the distal subaerial volcanic eruptions might be explained by the presence of QNC in BIF hematite. Recent studies have inventoried the frequency of subaerial volcanic activities during the transition from Archean to Palaeoproterozoic, which have been linked to the oxidation of atmosphere (Kasting et al., 1993; Barley et al., 2005; Holland, 2006; Kump and Barley, 2007). Consistent with the subaerial volcanic eruption scenario, tuffaceous mudrocks rich in stilpnomelane volcanoclastics have been reported in the vicinity of Dales Gorge BIF in the Hamersley Basin (Pickard, 2002; Trendall et al., 2004), indicating periods of episodic volcanism. The likelihood that (Si,Al)-containing flakes derived from the dissolution of the Al-containing stilpnomelane is not well-founded because bundles of acicular stilpnomelane of ~20μm in length were observed in some of the magnetite- and ankerite-rich thin mudrock layers in BIFs. The re-crystallization of amorphous silica to euhedral QNCs under diagenetic or metamorphic conditions does not seem plausible because no re-crystallization can be found in adjacent μm-bands of chert, neither in macrobands of chert alternate to the hematite bands. The much smaller crystal sizes of these QNCs and their unique morphology also makes them different from the authigenic euhedral quartz (a few μm) that can crystallize at ambient temperature (e.g., MacKenzie & Gees, 1971; Herdianita et al., 2000). For example, through interaction with an external thermal fluid, amorphous silica (and hematite) could recrystallize to much larger grains (>1 μm) under metamorphic conditions (<300ºC, Hippertt et al., 2001). On the contrary, the deposition of submicrometer airborne dusts, such as the volcanic nano-particles from the atmosphere diffused from distance could be a reasonable source of the pyroclastic-derived QNC materials. The riverine transport of terrestrial material is unlikely because there is no petrological evidence of the existence of weathering material, nor any hydrodynamic features in BIF (this study; Morris, 1993; Trendall, 2002).

The absence of QNC in other layers of Dales Gorge BIF suggests either a cessation of volcanism and/or widespread dispersion and dilution by the deep water. However, we still cannot exclude the precipitation of QNCs in some other BIFs, or even the other parts of the examined samples because the deposition of QNCs is a highly momentary event when compared to the long depositional history of BIFs. According to Trendall et al. (2004), the integrated depositional rate of Dales Gorge

BIF was about 5m per million years, which means the transition from the QNC-containing hematite to hematite without QNCs shown in Fig. 3L was only a matter of one year or so. Nevertheless, the presence of QNCs implies a hiatus between the precipitation of hematite and the formation of the other minerals in the BIF assemblage. In other words, the QNC became incorporated into the sediment during the earliest stages of diagenesis, and prior to the formation of later stage diagenetic or metamorphic minerals (e.g., magnetite and ferro-silicates). The Dales Gorge BIF, or more accurately, the hematite in it acted as a “repository” of QNCs derived from an airborne source, such as the eruption of local subaerial volcanoes (Pickard et al., 2004), because the transportation of authigenic quartz with weathered terrestrial source would preserve particles with varied size, possibly a somewhat rounded habit and complex mineralogy. This finding supports the contention that the Archean-Paleoproterozoic transition was a time when subaerial volcanism existed (Barley et al. 2005), and in this regard, we provide physical evidence in support of models that propose a link between changing tectonics, volcanism and the redox composition of gases emitted into the atmosphere (Barley et al., 1997; Kump et al., 2001; Barley et al., 2005; Kump and Barley, 2007).

ACKNOWLEDGEMENTS: YLL was supported by General Research Fund (HKU 703911) Research Grants Council of Hong Kong. KK acknowledges support from the Natural Sciences and Engineering Research Council of Canada. DRC was supported by a grant from the U.S. Department of Energy, Office of Basic Energy Sciences, Geoscience Research Program to Oak Ridge National Laboratory, which is operated by UT Battelle, LLC under Contract No. DE-AC05-00OR22725 for the U.S. Department of Energy. We thank Professor M. Darby Dyar for her great patience in editing and anonymous reviewers for their constructive reviews of our manuscript.

REFERENCES

Ahn, J.H. and Buseck, P.R. (1990) Hematite nanospheres of possible colloidal origin from a Precambrian banded iron formation. Science, 250, 111-113.

Barley, M.E., Bekker, A., Krapez, B. (2005) Late Archean to Early Paleoproterozoic global tectonics, environmental change and the rise of atmospheric oxygen. Earth and Planetary Science Letters, 238, 156-171.

Barley, M.E., Pickard, A.L., Sylvester P.J. (1997) Emplacement of a large igneous province as a possible course of banded iron formation 2.45 billion years ago. Nature, 385, 55-58.

Bau, M. and Dulski, P. (1996) Distribution of yttrium and rare-earth elements in the Penge and Kuruman Iron-Formations, Transvaal Supergroup, South Africa. Precambrian Research, 79, 37-55.

Campbell, I.H. and Allen C.M. (2008) Formation of supercontinents linked to increases in atmospheric oxygen. Nature Geoscience, 1, 554-558.

Eriksson, K.A. (1983) Siliciclastic-hosted iron-formations in the early Archaean Barberton and Pilbara sequences. Journal of the Geological Society of Australia, 30, 473-482.

Ewers, W.E. and Morris, R.C. (1981) Studies of the Dales Gorge Member of the Brockman iron formation, Western Australia. Economic Geology, 76, 1929-1953.

Fedo, C.M. and Eriksson, K.A. (1996) Stratigraphic framework of the ~3.0 Ga Buhwa greenstone belt: a unique stable-shelf succession in the Zimbabwe Archean craton. Precambrian Research, 77, 161-178.

Herdianita, N.R., Browne, P.R.L., Rodgers, K.A., Campbell, K.A. (2000) Mineralogical and textural changes accompanying ageing of silica sinter. Mineral Deposita, 35, 48-62.

Hippertt, J., Lana, C., Takeshita, T. (2001) Deformation partitioning during folding of banded iron formation. Journal of Structural Geology, 23, 819-834.

Holland, H.D. (2006) The oxygenation of the atmosphere and oceans. Philosophical Transactions of the Royal Society, B361, 903-916.

Kasting, J.F., Eggler, D.H., Raeburn, S.P. (1993) Mantle redox evolution and the oxidation state of the atmosphere. Journal of Geology, 101, 245-257.

Klein, C. (2005) Some Precambrian banded iron-formations (BIFs) from around the world: their age, geological setting, mineralogy, metamorphism, geochemistry, and origin. American Mineralogist, 90, 1473-1499.

Klein, C., and Ladeira, E.A. (2000) Geochemistry and petrology of some Proterozoic banded iron-formations of the Quadrilatero Ferrifero, Minas Gerais, Brazil. Economic Geology, 95, 405-428.

Knauth, L.P. (2005) Temperature and salinity history of the Precambrian ocean: implications for the course of microbial evolution. Palaeogeography, Palaeoclimatology, Palaeoecology, 219, 53-69.

Krapež, B., Barley, M.E., Kickard, A.L. (2003) Hydrothermal and resedimented origins of the precursor sediments to banded iron formation: sedimentological evidence from the Early Palaeoproterozoic Brockman Supersequence of Western Australia. Sedimentology, 50, 979-1011.

Kump, L.R., Barley, M.E. (2007) Increased subaerial volcanism and the rise of atmospheric oxygen 2.5 billion years ago. Nature, 448, 1033-1036.

Kump, L.R., Kasting, J.F., Barley, M.E. (2001) Rise of atmospheric oxygen and the "upside-down" Archean Mantle. Geochemistry Geophysics Geosystems, 2, Paper no. 2000GC000114.

La Berge, G.L. (1966) Altered pyroclastic rocks in iron-formation in the Hamersley Range, Western Australia. Economic Geology, 61, 147-161.

Li, Y.L., Konhuaser, K.O., Cole, D.R., Phelps, T.J. (2011) Mineral ecophysiological evidence for biogeochemical cycles in an early Paleoproterozoic banded iron formation. Geology, 39, 707-710.

MacKenzie, F.T. and Gees, R. (1971) Quartz: synthesis at Earth-surface conditions. Nature, 173, 533-535.

Morris, R.C. (1993) Genetic modeling for banded iron-formation of the Hamersley Group, Pilbara Craton, Western Australia. Precambrian Research, 60, 243-286.

Pecoits, E., Gingras, M.K., Barley, M.E., Kappler, A., Posth, N.R., Konhauser, K.O. (2009) Petrography and geochemistry of the Dales Gorge banded iron formation: paragenetic sequence, source and implications for palaeo-ocean chemistry. Precambrian Research, 172, 163-187.

Pickard, A.L. (2002) SHRIMP U-Pb zircon ages of tuffaceous mudrocks in the Brockman iron formation of the Hamersley Range, Western Australia. Australian Journal of Earth Sciences, 49, 491-507.

Pickard, A.L., Barley, M.E., Krapez, B. (2004) Deep-marine depositon setting of banded iron formation: sedimentological evidence from interbedded clastic sedimentary rocks in the early Palaeoproteroaoic Dales Gorge Member of Western Australia. Sedimentary Geology, 170, 37-62.

Schneider, D.A., Bickford, M.E., Cannon, W.F., Schulz, K.J., Hamilton, M.A. (2000) Age of volcanic rocks and syndepositional iron formations, Marquette Range Supergroup: implications for the tectonic setting of Paleoproterozoic iron formations of the Lake Superior region. Canadian Journal of Earth Sciences, 39, 999-1012.

Trendall, A.F. (2002) The significance of iron-formation in the Precambrian stratigraphic record. In W. Altermann, and P.L. Corcorane Eds., Precambrian Sedimentary Environments: a Modern Approach to Depositional System, 33-66, Oxford, Blackwell Publishing Ltd.

Trendall, A.F., and Blockley J.G. (1970) The iron formation of the Precambrian Hamersley Group, Western Australia. Geological Survey of Western Australia Bulletin, 119, pp 365.

Trendall, A.F., Compston, W., Nelson, D.R., De Laeter, J.R., Bennett, V.C. (2004) SHRIMP zircon ages constraining the depositional chronology of the Hamersley Group, Western Australia. Australian Journal of Earth Sciences, 51, 621-644.

Zhai, M., and Windley, B.F. (1990) The Archaean and early proterozoic banded iron formations of North China: their characteristics, geotectonic relations, chemistry and implications for crust growth. Precambrian Research, 48, 267-286.

Figure captions

Figure 1. The chert (amorphous silica) and hematite bands in BIF. (A) the BSE mode image of chert (dark) and hematite (grey). The magnetite crystals (white) are disseminated in the matrix of chert and hematite; (B) feature of silica polyhedrons; (C) hematite surface with depressions of several μm in size; (D) the BSE image of anhedral hematite showing imbedded silica nodules and pits produced by magnetite crystals; (E) the aggregates of platy hematite; (F) the eroded landform-like surface of an anhedral particle.

Figure 2. High resolution TEM image of the ultrafine hematite crystals (A) and the SAED determined structure of hematite (B).

Figure 3. Euhedral QNCs and Al-containing flakes on the surface or in the hematite breccias. (A) a surface of hematite flake showing deposition of QNCs on the surface; (B) two QNCs amplified from the upper right of image (A); (C) a QNC on the surface of hematite with falling scratches; (D) a QNC similar to (C) with a nearby empty pit; (E) A QNC amplified from the lower right part of image (A); (F) a QNC in one deep pit; (G-J) various surfaces of hematite showed the existence of QNCs inside the hematite breccias; (K) a hematite breccia containing QNCs only in its low-left part but no QNC in its upper-left part; (L) the surface of hematite showed the co-existences of QNC and flake-like crystals of similar size.

Figure 4. The chemical compositions of QNC and (Si, Al)-containing nanocrystals. (A) the surface of hematite containing QNCs for EDS analysis; (B) the EDS analysis showed a small Si-peak besides Fe- and O-peaks; (C) the thin flakes in cavities (arrowed); (D) the EDS analysis of arrowed spots in image (C) showed Si and Al peaks besides Fe- and O-peaks.

Figure 5. STEM determination of the structure of QNC. (A) QNC (bottom right) in the residue of the 6M-HCl treated hematite; (B) the SAED of QNC in A observed from zone axis of [421] indicated the structure of well-crystallized quartz; (C) chert microcrystallites under STEM; (D) the SAED pattern of chert in image (C) revealed their amorphous nature.

Figure 6. Selected hematite from BIF of different ages showing no QNC during their formations. (A) 1.8 Ga BIF from North China (Zhai & Windley, 1990); (B) Michigan, 1874 Ma (Schneider et al., 2000); (C) Brazil, 2.4 Ga (Klein & Ladeira, 2000); (D) 2.52 Ga BIF from North China (Zhai & Windley, 1990); (E) South Africa, 3.0-3.3 Ga, (Eriksson, 1983); (F) BIF from Zimbabwe, ~3.0 Ga (Fedo & Eriksson, 1996).

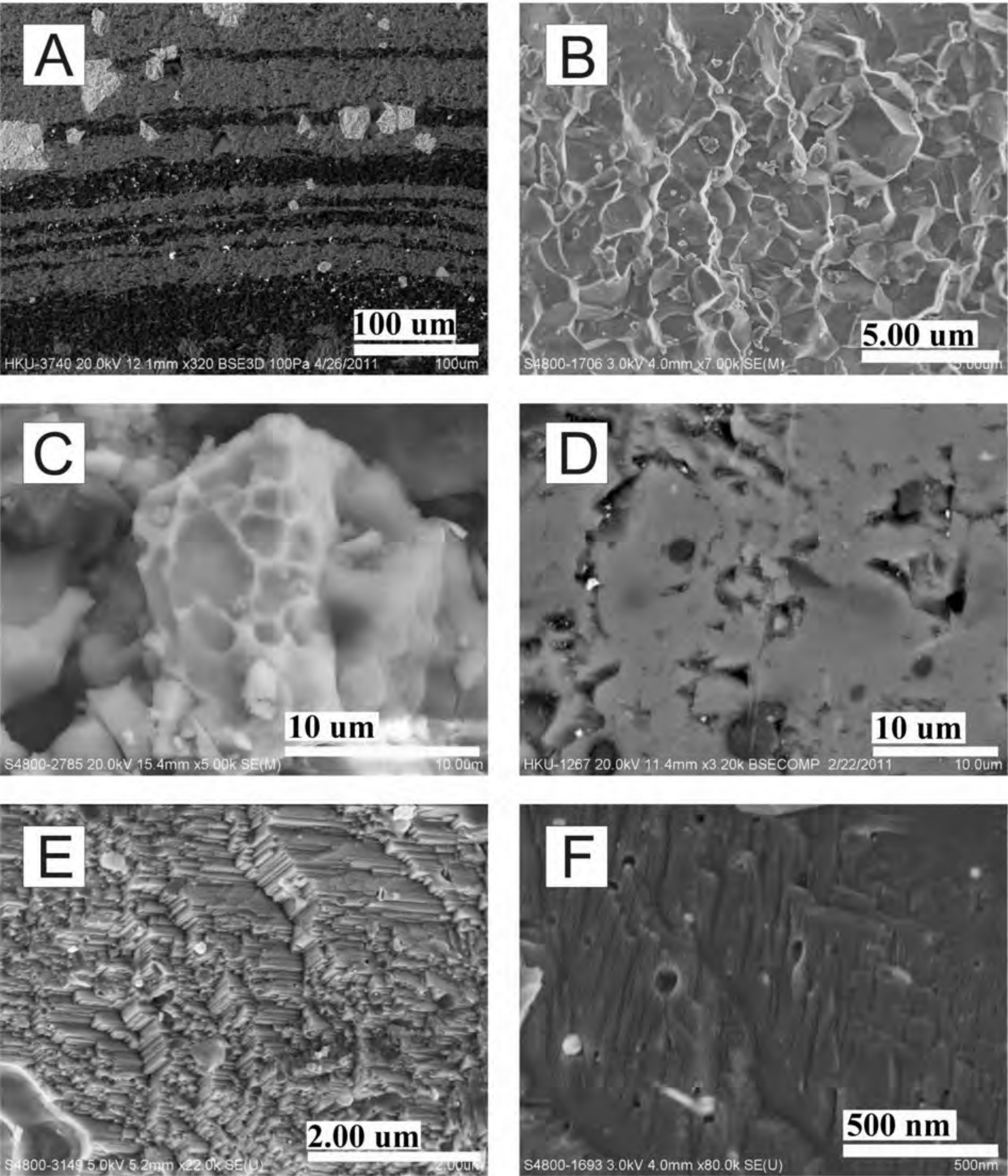

A
100 um
HKU-3740 20.0kV 12.1mm x320 BSE3D 100Pa 4/26/2011
100um
B
5.00 um
S4800-1706 3.0kV 4.0mm x7.00k SE(M)
C
10 um
S4800-2785 20.0kV 15.4mm x5.00k SE(M)
10.0um
D
10 um
HKU-1267 20.0kV 11.4mm x3.20k BSECOMP 2/22/2011
10.0um
E
2.00 um
S4800-3149 5.0kV 5.2mm x22.0k SE(U)
F
500 nm
S4800-1693 3.0kV 4.0mm x80.0k SE(U)
500nm

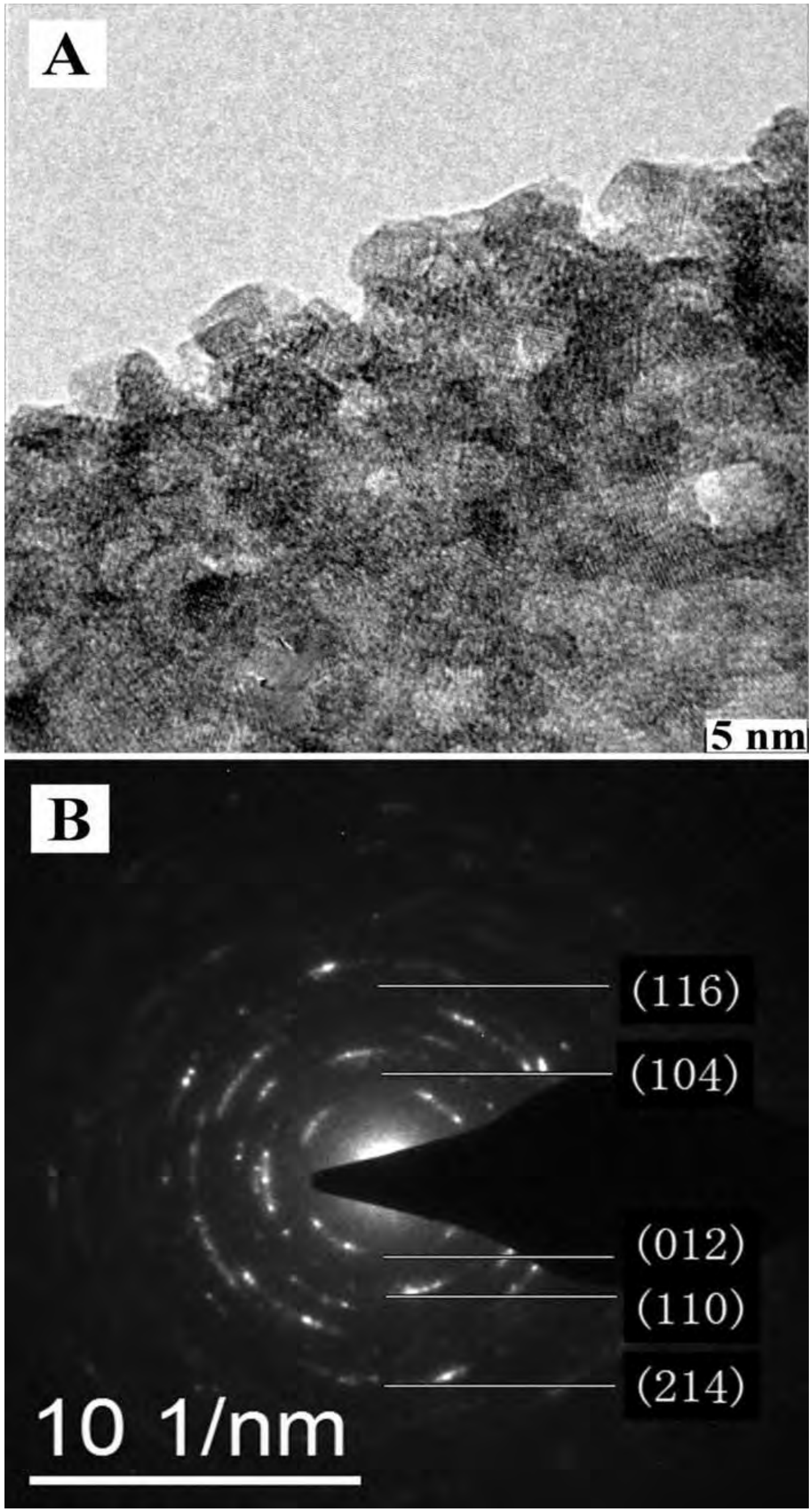
A
5 nm
B
(116)
(104)
(012)
(110)
(214)
10 1/nm

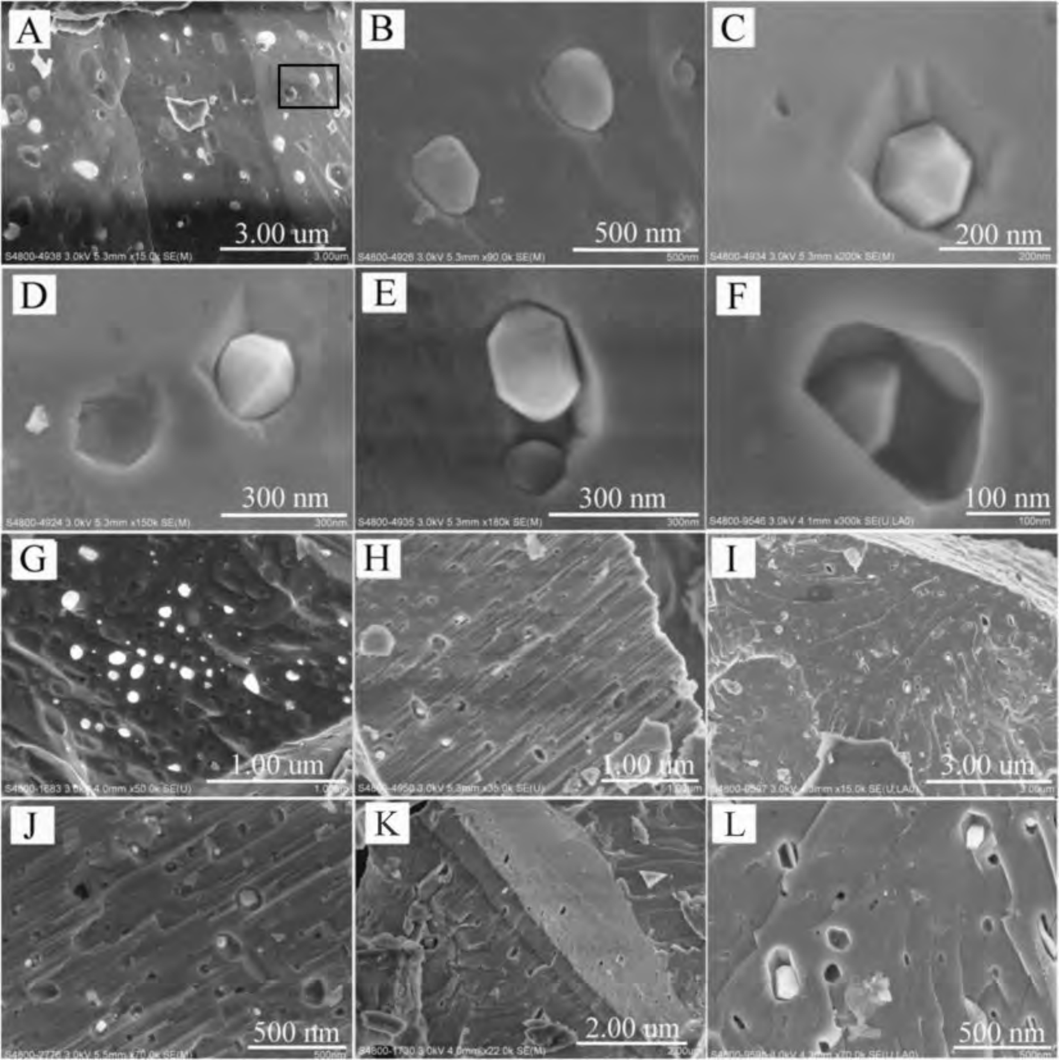
A
3.00 um
B
500 nm
C
200 nm
D
300 nm
E
300 nm
F
100 nm
G
1.00 um
H
1.00 um
I
3.00 um
J
500 nm
K
2.00 um
L
500 nm

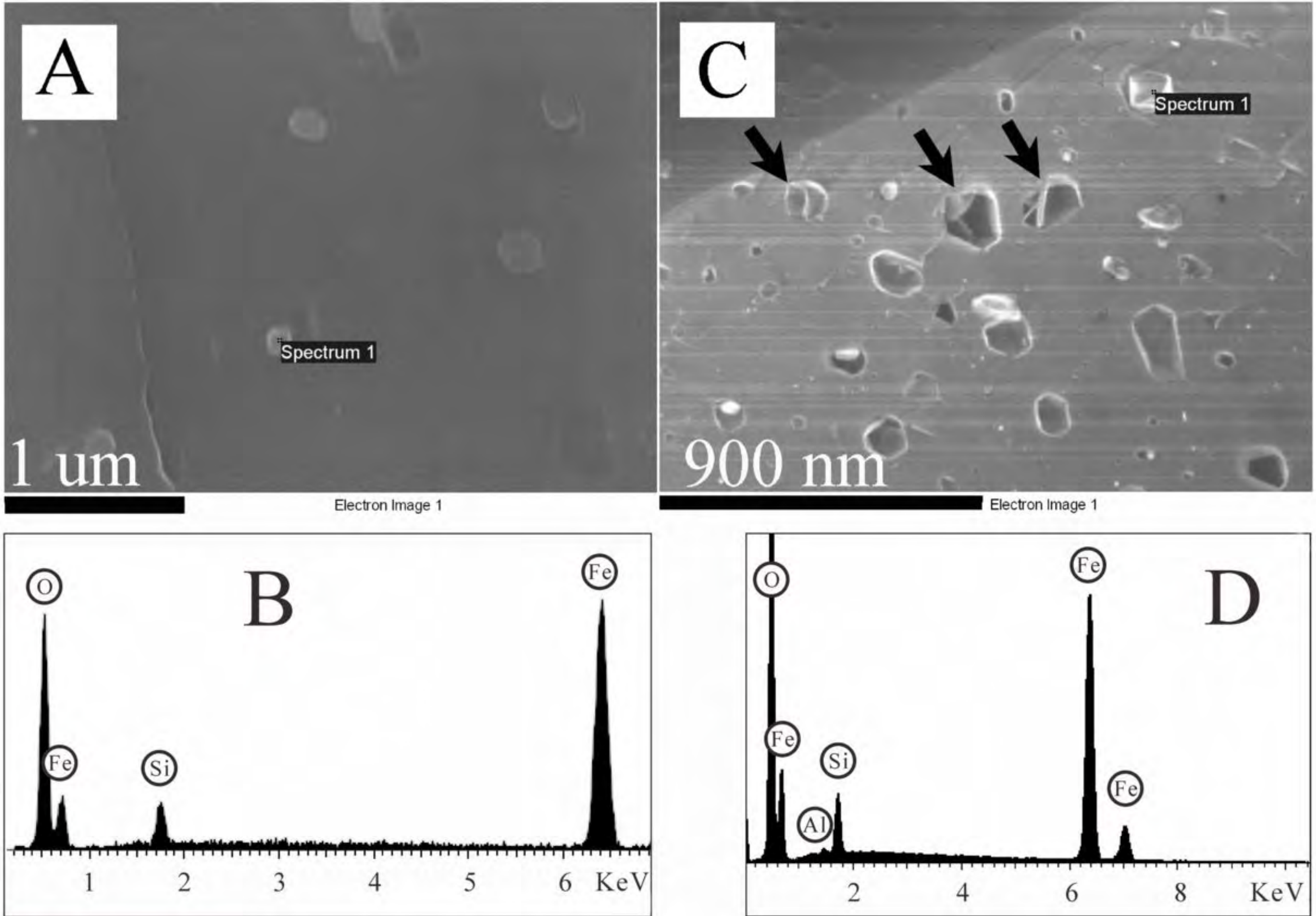

A
Spectrum 1
1 um
Electron Image 1
C
Spectrum 1
900 nm
Electron Image 1
B
O
Fe
Si
Fe
1
2
3
4
5
6
KeV
D
O
Fe
Al
Si
Fe
Fe
2
4
6
8
KeV

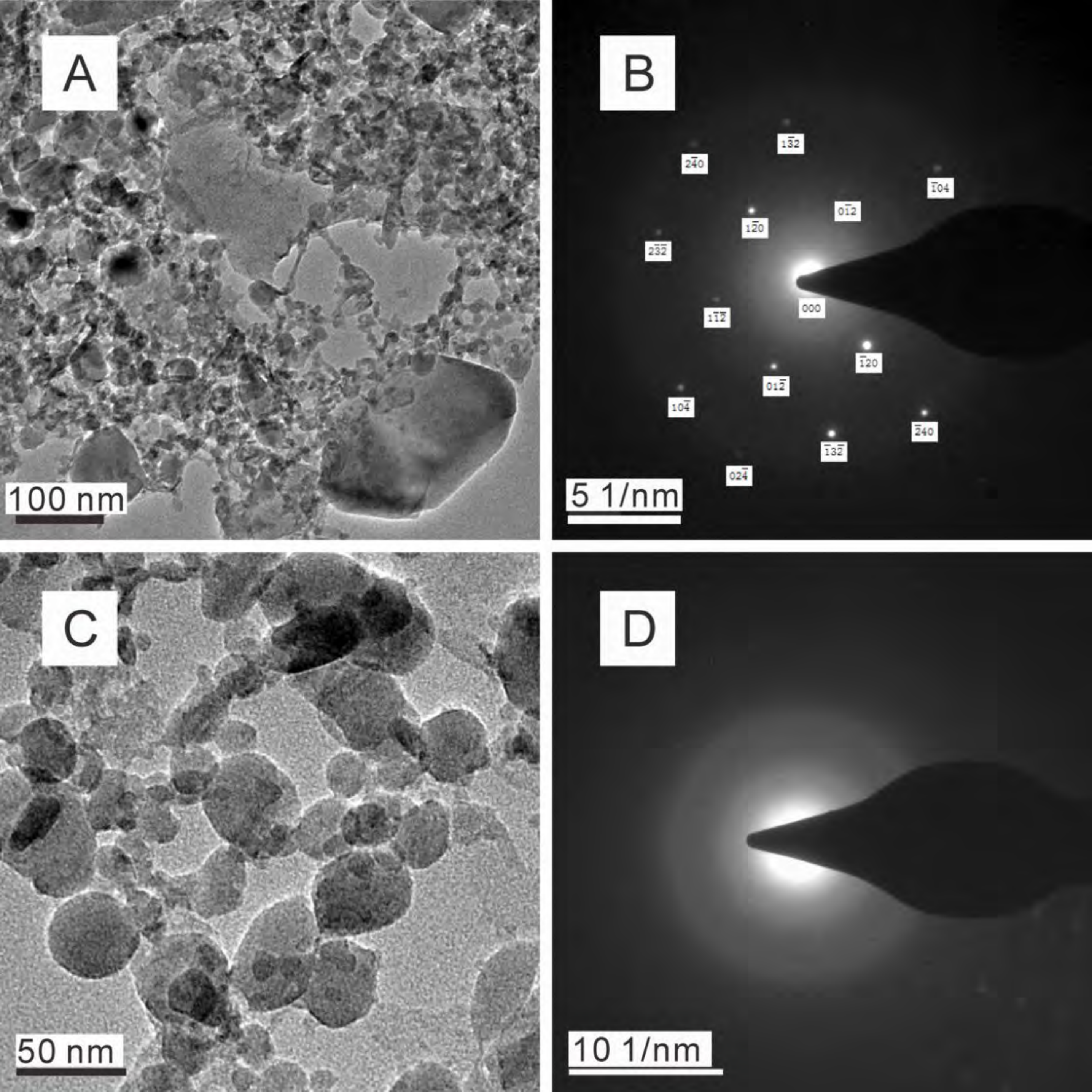
A
100 nm
B
$1\bar{3}2$
$2\bar{4}0$
$\bar{1}04$
$0\bar{1}2$
$1\bar{2}0$
$2\bar{3}\bar{2}$
000
$1\bar{1}\bar{2}$
$\bar{1}20$
$01\bar{2}$
$10\bar{4}$
$\bar{2}40$
$\bar{1}3\bar{2}$
$02\bar{4}$
5 1/nm
C
50 nm
D
10 1/nm

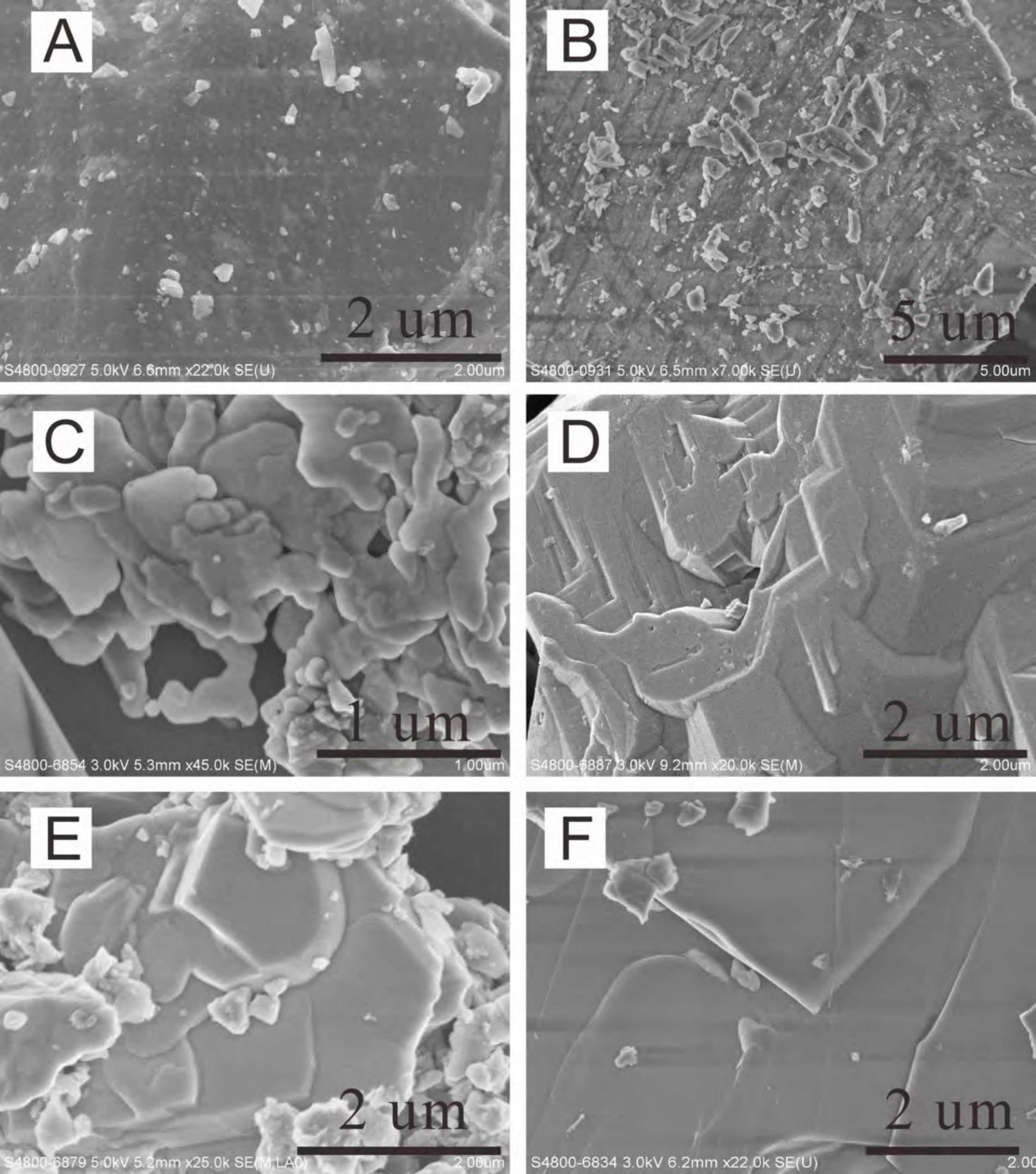
A
2 um
S4800-0927 5.0kV 6.6mm x22.0k SE(U)
2.00um
B
5 um
S4800-0931 5.0kV 6.5mm x7.00k SE(U)
5.00um
C
1 um
S4800-6854 3.0kV 5.3mm x45.0k SE(M)
1.00um
D
2 um
S4800-6887 3.0kV 9.2mm x20.0k SE(M)
2.00um
E
2 um
S4800-6879 5.0kV 5.2mm x25.0k SE(M,LA0)
2.00um
F
2 um
S4800-6834 3.0kV 6.2mm x22.0k SE(U)